Spatial frequency maps of power flow in metamaterials and photonic crystals: Investigating backward-wave modes across the electromagnetic spectrum

Iman Aghanejad and Loïc Markley[*]

School of Engineering, University of British Columbia, Kelowna, BC, Canada

We present spatial frequency maps of power flow in metamaterials and photonic crystals in order to provide insights into their electromagnetic responses and further our understanding of backward power in periodic structures. Since 2001, many different structures across the electromagnetic spectrum have been presented in the literature as exhibiting an isotropic negative effective index. Although these structures all exhibit circular or spherical equifrequency contours that resemble those of left-handed media, here we show through k-space diagrams that the distribution of power in the spatial frequency domain can vary considerably across these structures. In particular, we show that backward power arises from high-order right-handed harmonics in photonic crystals, magnetodielectric crystals, and across the layers of coupled-plasmonic-waveguide metamaterials, while arising from left-handed harmonic pairs in split-ring resonator and wire composites, plasmonic crystals, and along the layers of coupled-plasmonic-waveguide metamaterials. We also show that the fishnet structure exhibits the same left-handed harmonic pairs as the latter group. These observations allow us to categorize different metamaterials according to their spatial spectral source of backward power and identify the mechanism behind negative refraction at a given interface. Finally, we discuss how k-space maps of power flow can be used to explain the high or low transmittance of power into different metamaterial or photonic crystal structures.

I. INTRODUCTION

Over four decades ago, Veselago proposed that an isotropic and homogeneous double-negative medium (with simultaneously negative values of ϵ and μ) could theoretically sustain left-handed plane waves with antiparallel phase and energy velocities [1]. This would imply that the equifrequency contours (EFCs), which are traced out by the wave vectors in k space at each frequency, would be spheres whose frequency gradient (the group velocity) points inwards everywhere over their surfaces. This extraordinary property (unobserved in natural materials) can be completely characterized by a three-dimensionally isotropic negative refractive index and has been predicted to result in many interesting phenomena such as negative refraction and perfect imaging [1,2].

Although backward modes (in which energy flows in the opposite direction to the wavefronts) have long been observed in transmission-line and waveguide structures [3,4], negative refraction and perfect imaging require bulk media with two or three-dimensional isotropy. Artificial structures known as metamaterials and photonic crystals have been proposed and fabricated in order to implement such negative effective index media from microwave to optical frequencies [5–9]. These subwavelength periodic structures are able to support propagating backward Bloch modes in which the time-and-space-averaged Poynting vector **S** and the Floquet-Bloch wave vector $\mathbf{k}_{FB}$ are in opposite directions. Through careful design, this behavior can be preserved for all directions of propagation in a two-dimensional plane or in three-dimensional space resulting in nearly circular or spherical EFCs resembling that of an isotropic left-handed Veselago medium. If we consider only the average power and Floquet-Bloch wave vector [located in the first Brillouin zone (BZ)], these circular EFCs imply that a 2D or 3D left-handed response can be mimicked and that

negative refraction of both power and phase would be feasible. Experiments showing negative refraction of electromagnetic beams have been used as corroborating evidence of a left-handed response and has led to the general characterization of these structures as isotropic negative-index media. In this work, we assess the validity of these characterizations.

Homogenization approximations have been widely used to model negatively refracting periodic structures by homogeneous media with double-negative effective constitutive parameters (or equivalently, negative effective index n_{eff} and effective impedance η_{eff}) [10–14]. These models effectively map backward Bloch modes to single left-handed plane waves located in the first BZ. With this mapping, however, important information about the behavior of EM fields inside the medium can be hidden and the validity of effective medium models cannot be guaranteed in a general periodic structure.

It has been shown using spatial frequency maps of power flow that the fundamental harmonic of a Bloch mode (which has a wave vector equal to $\mathbf{k}_{FB}$) can have a nonsignificant contribution to the total power flow with most of the power carried outside the first BZ [15–18]. Spatial frequency maps are formed by decomposing the electric and magnetic Bloch-mode fields into complete sets of spatial frequency harmonics and plotting the corresponding Poynting vectors in k space. This provides a simple visual representation of the electromagnetic behavior based off a systematic and general procedure that can be applied to any periodic structure, regardless of frequency, periodicity, or constituent materials. For example, in Ref. [17], we investigated a coupled-plasmonic-waveguide metamaterial, which had been characterized by a three-dimensionally isotropic effective negative refractive index $n = -1$. Although this structure achieves a nearly spherical EFC and demonstrates wide-angle negative refraction of light beams, we showed that the spatial frequency distribution of power flow is revealed to be strongly anisotropic and that the spatial frequency origin of backward power evolves from pairs

---
[*]loic.markley@ubc.ca

of left-handed harmonics for propagation along the layers to higher-order right-handed harmonics for propagation across the layers. This identification of the dominant harmonics (i.e., those with significant contributions to the total power flow) enabled us to determine the spatial frequency origin of observed negative refraction and predict alternative wave excitations to better couple power into the structure. For example, we showed that negative refraction at the interface parallel to the layers originates from the refraction of higher-order right-handed components, not from left-handedness. In addition, we showed that exciting the dominant higher-order power harmonics rather than the fundamental harmonic at the interface perpendicular to the layers could increase the coupling efficiency by a factor of five. These findings revealed the limitations of relying on EFC analysis alone to characterize the response of a metamaterial or photonic crystal and demonstrated the importance of first considering the spatial-frequency power distribution when attempting to use the Bloch impedance to model wave propagation across the interface of a general periodic structure.

In this paper, we apply k-space analysis to several common metamaterials and photonic crystals that have been described in the literature as negative index media. Mapping the complete power distribution of spatial frequency harmonics provides new insights into the behavior of propagating modes, enabling us to identify the spatial frequency origin of backward power and distinguish between the electromagnetic responses of structures with similar EFCs. Since heterogeneous structures can only mimic the electromagnetic behavior of left-handed media, spatial spectral power maps can be used to provide a quantitative comparison with an ideal left-handed medium in order to compare and contrast different metamaterials across the electromagnetic spectrum. We will show that the source of backward power in metamaterials and photonic crystals arises primarily from either higher-order right-handed harmonics or from pairs of left-handed waveguide modes. In other words, we can use the spatial frequency maps of power flow as a signature to categorize different structures that carry backwards power. The knowledge of how power is distributed in k space provides an explanation for why some periodic structures can exhibit all-angle negative refraction of power despite the lack of a left-handed response. It also reveals why an incident plane wave that is phase and impedance matched to the effective medium parameters does not necessarily result in high transmission into a periodic structure.

The remainder of the paper is divided into eight sections. In the next section, we present a general method to analyze periodic structures based on their spatial power harmonics. The next six sections apply this method to a split-ring resonator and thin-wire composite, a photonic crystal, a magnetodielectric crystal, a plasmonic crystal, a coupled-plasmonic-waveguide metamaterial, and a fishnet structure. The spatial frequency power maps are compared and similar features are highlighted. The final section concludes the paper and summarizes our findings.

II. METHODOLOGY

In order to calculate the power distribution of a backward Bloch mode over k space, we must first determine the electric

and magnetic fields of that mode. The Floquet-Bloch theorem [19,20] states that electric and magnetic fields in an infinite and periodic structure have the form of

$$\mathbf{E}(\mathbf{r},t) = \mathbf{u_e}(\mathbf{r})e^{i(\mathbf{k}_{FB}\cdot\mathbf{r}-\omega t)}, \tag{1}$$

$$\mathbf{H}(\mathbf{r},t) = \mathbf{u_h}(\mathbf{r})e^{i(\mathbf{k}_{FB}\cdot\mathbf{r}-\omega t)}, \tag{2}$$

where $\mathbf{u_e}(\mathbf{r})$ and $\mathbf{u_h}(\mathbf{r})$ are periodic vector functions with the same periodicity as the medium, ω is the frequency, and $\mathbf{k}_{FB}$ is the Floquet-Bloch wave vector (located in the first BZ) which can generally be complex and expressed as $\mathbf{k}_{FB} = \mathbf{k} + i\boldsymbol{\alpha}$. The real part $\mathbf{k}$ is the fundamental propagating wave vector and the imaginary part $\boldsymbol{\alpha}$ is the attenuation vector. As the attenuation is embedded in the complex Floquet-Bloch wave vector, the vector functions $\mathbf{u_e}(\mathbf{r})$ and $\mathbf{u_h}(\mathbf{r})$ always represent the nonattenuating periodic component of $\mathbf{E}(\mathbf{r},t)$ and $\mathbf{H}(\mathbf{r},t)$, respectively. The Bloch modes supported by the periodic structure can be determined by solving the Helmholtz equation as an eigenvalue problem at fixed frequencies. Substitution of Eqs. (1) and (2) into the Helmholtz equation yields

$$\nabla \times \left(\frac{1}{p}\nabla \times \mathbf{u}\right) + i\mathbf{k}_{FB} \times \left(\frac{1}{p}\nabla \times \mathbf{u}\right)$$
$$+ i\nabla \times \left(\frac{1}{p}\mathbf{k}_{FB} \times \mathbf{u}\right)$$
$$+ \frac{\mathbf{k}_{FB}\cdot\mathbf{k}_{FB}}{p}\mathbf{u} - \frac{\mathbf{k}_{FB}}{p}(\mathbf{k}_{FB}\cdot\mathbf{u}) - q\frac{\omega^2}{c^2}\mathbf{u} = 0, \tag{3}$$

where $\mathbf{u} = \mathbf{u_e}$, $p = \mu$, and $q = \varepsilon$ for the electric field and $\mathbf{u} = \mathbf{u_h}$, $p = \varepsilon$, and $q = \mu$ for the magnetic field [21]. Here, μ and ε are the relative permeability and permittivity of the periodic medium, respectively, both of which can be complex and dispersive in general. In order to solve this equation as an eigenvalue problem at a fixed frequency, constraints must be placed on the Floquet-Bloch wave vector $\mathbf{k}_{FB}$ so that it can be expressed in terms of a single scalar eigenvalue λ. Different constraints can be used for different circumstances, with the corresponding eigensolutions unique only to that constraint. In the case of the infinite periodic structures studied in this paper, we apply a constraint by defining a direction of propagation and choose $\mathbf{k}_{FB} = \lambda\hat{\mathbf{k}}$. Equation (3) can be solved over a single unit cell for the complex eigenvalue λ and its corresponding eigenmode $\mathbf{u}(\mathbf{r})$ in order to compare the electromagnetic response in different directions of propagation. The EFC associated with a particular frequency is then given by tracing the Floquet-Bloch wave vector across all directions of propagation. Note that since this formulation is evaluated at a single frequency, dispersive materials can be treated in the same manner as nondispersive materials. In this work, we solved the weak form of the eigenvalue equation (3) for $\mathbf{u_e}$ or $\mathbf{u_h}$ using COMSOL MULTIPHYSICS finite-element software package [21,22].

It has often been assumed that when the periodicity is subwavelength, the Bloch mode can be approximated by a single plane wave with the wave vector $\mathbf{k}_{FB}$ [see Eqs. (1) and (2)]. This has led to the modeling of metamaterials and photonic crystals by equivalent homogeneous media (using effective parameters) [10–14,23] or by repeated zone EFC

diagrams [9,24]. The periodicity of the EFCs in the spatial frequency domain, however, has been shown to lead to an ambiguity in assigning a single wave vector (i.e., a single phase velocity) to the propagating mode [15,17,18]. This ambiguity implies that the feasibility of modeling the propagating modes with a single plane wave inside the first BZ is not guaranteed in periodic structures and hence their characterization by effective parameters or dispersion diagrams alone can be misleading.

Instead, a complete description of Floquet-Bloch modes that retains all spatial field information can be achieved by expanding the electric and magnetic fields into a complete set of spatial frequency harmonics as follows:

$$\mathbf{H}(\mathbf{r}) = \sum_{l,m,n} \mathbf{h}_{l,m,n} e^{i\mathbf{G}_{l,m,n}\cdot\mathbf{r}} e^{i\mathbf{k}_{\mathrm{FB}}\cdot\mathbf{r}}, \tag{4}$$

$$\mathbf{E}(\mathbf{r}) = \sum_{l,m,n} \mathbf{e}_{l,m,n} e^{i\mathbf{G}_{l,m,n}\cdot\mathbf{r}} e^{i\mathbf{k}_{\mathrm{FB}}\cdot\mathbf{r}}, \tag{5}$$

where $\mathbf{G}_{l,m,n}$ is the reciprocal vector and l, m, n span the set of all integers. In this formulation, $\mathbf{h}_{l,m,n}$ and $\mathbf{e}_{l,m,n}$ are the three-dimensional spatial Fourier transforms of the nonattenuating periodic components of the magnetic and electric field vectors, respectively. The harmonic components of the electric and magnetic fields each have a real wave vector given by $\mathbf{k}_{l,m,n} = \mathbf{k} + \mathbf{G}_{l,m,n}$ and an attenuation vector given by $\boldsymbol{\alpha} = \mathrm{Im}\{\mathbf{k}_{\mathrm{FB}}\}$. By pairing corresponding electric and magnetic field harmonics, the Bloch mode can be expressed as a spectrum of unique plane waves located at discrete real $\mathbf{k}_{l,m,n}$ points in the spatial frequency domain (k space). The time-averaged Poynting vector associated with each (nonattenuating) plane wave can be calculated using the following expression:

$$\mathbf{S}_{l,m,n} = \tfrac{1}{2}\,\mathrm{Re}\{\mathbf{e}_{l,m,n} \times \mathbf{h}_{l,m,n}^*\}. \tag{6}$$

Each plane-wave harmonic therefore has a well-defined wave vector $\mathbf{k}_{l,m,n}$ and Poynting vector $\mathbf{S}_{l,m,n}$ from which handedness can be defined. To calculate each harmonic's handedness, the wave vector and Poynting vector are projected onto a reference axis defined by the direction of propagation $\hat{\mathbf{k}}$. If the projected vectors are parallel (in the same direction), the harmonic is considered to be right handed, while if they are antiparallel (in the opposite direction), the harmonic is considered to be left handed. This generalizes the definition of handedness for individual harmonics from definitions that rely only on the direction of average power flow [25]. Consequently, since we use individual harmonic Poynting vectors to determine the direction of harmonic power flow (which can differ from the direction of average power flow), the sign relation between the real and imaginary components of a complex harmonic wave vector (in periodic structures with absorbing materials) no longer provides a sufficient criterion for determining the handedness of that harmonic.

Due to the orthogonality of the harmonics, the individual harmonic Poynting vectors can be related to the total time- and space-averaged Poynting vector through the following summation:

$$\mathbf{S} = \frac{1}{V}\int_V \frac{1}{2}\,\mathrm{Re}\{\mathbf{u}_e(\mathbf{r}) \times \mathbf{u}_h^*(\mathbf{r})\}dv = \sum_{l,m,n} \mathbf{S}_{l,m,n}, \tag{7}$$

where V is the volume of the unit cell. Rather than being confined to the first BZ, we can now map the total power flow across all spatial frequency harmonics for a complete characterization of the relationship between phase and power flow in periodic structures. This mapping can reveal cases where most of the power lies outside the first BZ, or reveal whether the power is carried primarily by right-handed or left-handed harmonics.

Note that in a general heterogeneous medium, handedness can be defined for individual harmonics but not for the medium itself. This is because a consistent phase progression typically does not exist when a medium is not homogeneous in the direction of propagation [17]. We must therefore refrain from associating any kind of handedness to the relative orientations of $\mathbf{k}_{\mathrm{FB}}$ and $\mathbf{S}$ (or equivalently, to the complex sign relation of $\mathbf{k}_{\mathrm{FB}}$) and discuss only the handedness of harmonics which can be determined using the method described above.

This method provides a systematic and generalized spatial frequency analysis that can be applied to arbitrary periodic structures (with dielectric, magnetic, and conductive modulations) under arbitrary polarization. In the following sections, this method is applied to several common metamaterials and photonic crystals to carefully investigate wave behavior that has been described in the literature as arising from negative refractive index.

## III. SPLIT-RING RESONATOR AND THIN-WIRE METAMATERIAL

The first experimental demonstration of negative refraction was performed at microwave frequencies using a composite metamaterial consisting of arrays of split-ring resonators (SRRs) and thin wires (TWs) [5,26]. In these experiments, measured refraction angles were shown to be consistent with Snell's law when the structure was modeled using a double-negative homogeneous and isotropic effective medium [27,28]. Negative effective permeability μ was attributed to out-of-phase magnetic moments induced within the SRRs [29], while negative permittivity ϵ was attributed to the plasmalike behavior of the thin-wire arrays [30].

Here, we apply the k-space analysis to provide new insights into the response of the SRR-TW structure. We consider a two-dimensional array of thin wires aligned with the z axis interspaced between two orthogonal arrays of SRRs and consider propagation parallel to the xy plane. The lattice has a periodicity a in the x and y directions and a periodicity $d = 0.86a$ in the z direction. The SRRs and thin wires are modeled as perfect electric conductors (PECs) with radii of $0.016a$ and $0.02a$, respectively. The SRRs embedded within crossed dielectric layers of permittivity $\varepsilon = 7$ and thickness $0.1a$. Each unit cell contains two complete SRRs (oriented orthogonally to each other) and one complete thin wire, as illustrated in the inset diagrams of Fig. 1.

We begin our study by solving the eigenvalue equation (3) to find the Bloch mode periodic function $\mathbf{u_h}(\mathbf{r})$ and the Floquet-Bloch wave vector $\mathbf{k}_{\mathrm{FB}}$ associated with each direction of propagation. Once $\mathbf{u_e}(\mathbf{r})$ is calculated from $\mathbf{u_h}(\mathbf{r})$, both periodic functions are expanded to their Fourier harmonics and each harmonic Poynting vector is then calculated. Figures 1 and 2 plot the harmonic Poynting vectors alongside the EFC contours
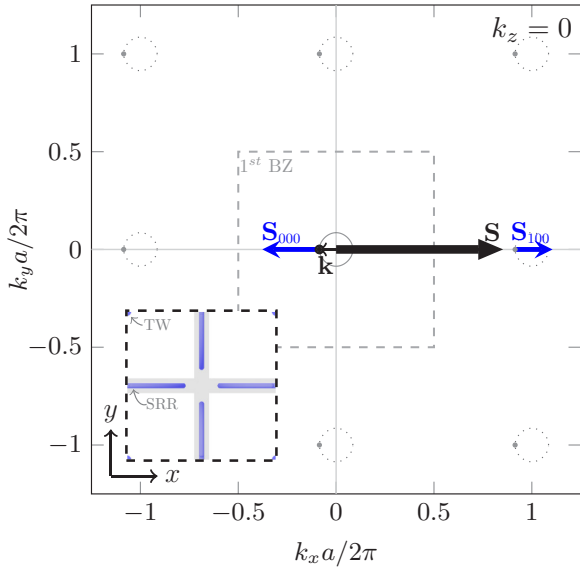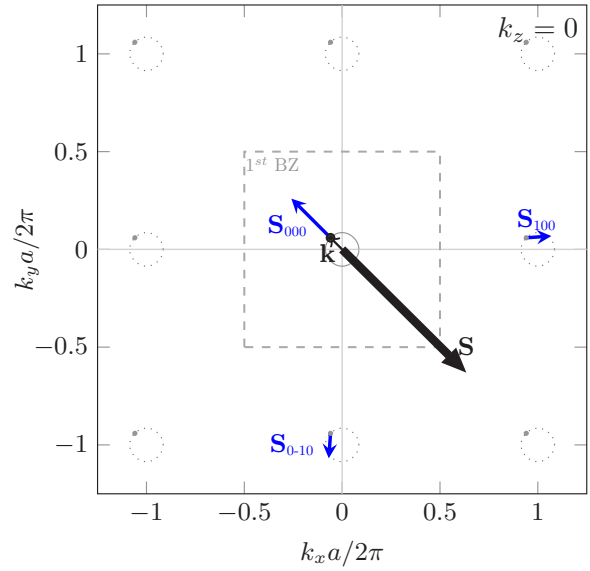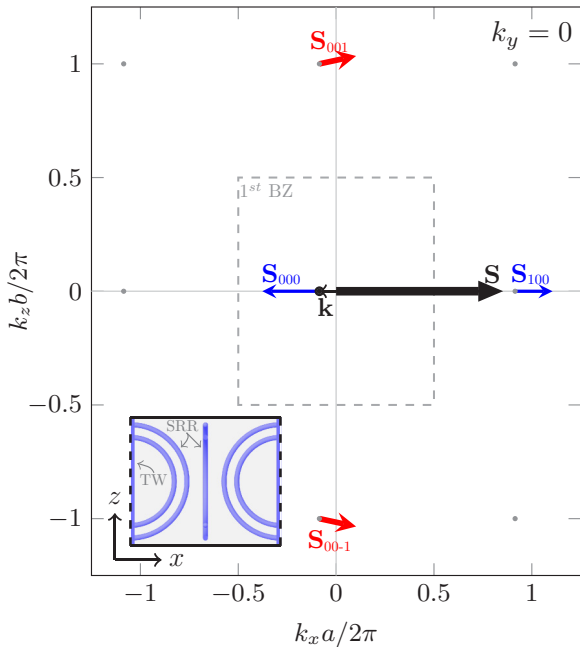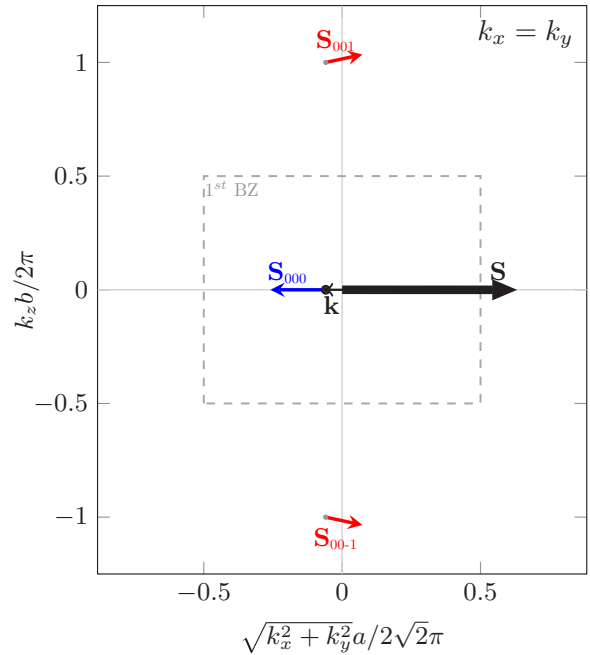
FIG. 1. The k-space diagrams for a backwards eigenmode propagating in-plane along the x axis of the SRR-TW metamaterial ($\phi = 0$). The Bloch harmonics are plotted on the $k_z = 0$ plane (a) and on the $k_y = 0$ plane (b). Left-handed plane-wave components in k space are plotted with red arrows, while right-handed components are plotted with blue arrows. The EFCs are given by the solid and dotted curves inside and outside the first BZ, respectively, where the first BZ is indicated by the light grey dashed rectangle. The unit cell is shown from the top (a, inset) and side (b, inset) with PEC boundary conditions (solid lines) in the z direction and periodic boundary conditions (dashed lines) in the x and y directions.

FIG. 2. The k-space diagrams for a backwards eigenmode propagating in-plane along the diagonal axis of the SRR-TW metamaterial ($\phi = 45°$). The Bloch harmonics are plotted on the $k_z = 0$ plane (a) and on the $k_x = k_y$ plane (b). Note that only the average power **S** must be normal to the EFC. Individual harmonic Poynting vectors are free to point in any direction.

of the structure for Bloch waves propagating parallel to and diagonally to the in-plane axes, respectively. The normalized

frequency of operation is $\Omega = a/\lambda_0 = 0.0647$, where λ_0 is the wavelength in free space. The time-and-space-averaged Poynting vector **S** of the global fields calculated by Eq. (7) is shown by the thick black arrow with the fundamental wave vector shown by the thin black arrow. The location of the fundamental harmonic is also indicated by a black dot. Note that unlike the total power flow **S**, the individual harmonic

Poynting vectors $\mathbf{S}_{l,m,n}$ are not necessarily normal to their corresponding repeated EFCs.

In conventional EFC analysis, the Bloch mode is modeled as a single plane wave located within the first BZ and no information about the harmonic distribution of power is available. Observing that the average power flow points opposite to the fundamental wave vector would therefore seem to imply a left-handed response characterized by a single negative refractive index. By plotting the harmonic Poynting vectors in the spatial frequency domain, however, information is provided about the Bloch mode field variations across each unit cell that is not available from EFC diagrams nor from effective parameters. We can see from Figs. 1 and 2 that the electromagnetic fields are a strong mixture of Bloch harmonics, containing both left-handed harmonics (in red) and right-handed harmonics (in blue), with only a fraction of the total power residing within the first BZ (i.e., residing within the fundamental).

The dominant harmonics in Fig. 1 can be separated into two distinct sets: the right-handed components are arranged longitudinally along the axis of propagation while the left-handed components are arranged in the transverse direction along an axis perpendicular to the direction of propagation. We will show later that this distribution of right and left handed components is not unique to this Bloch mode. The presence of one or both of these harmonic sets can reveal the spatial frequency origin of backward power in metamaterials and photonic crystals. Let us now explore each of these harmonic sets further.

The left-handed transverse harmonics $\mathbf{S}_{0,0,1}$ and $\mathbf{S}_{0,0,-1}$ shown in Fig. 1(b) can be interpreted as two plane waves bouncing back and forth within the parallel-plate waveguide formed by the unit cell PEC symmetry planes. These higher harmonics are symmetric with respect to the $k_x k_y$ plane and form standing waves in the direction transverse to the plane and propagating waves in the direction parallel to the plane. Together they form a backward "waveguide" mode in which power flows in the direction opposite to phase. As the direction of propagation changes in the xy plane, these left-handed harmonic pairs rotate about the k_z axis to maintain their transverse position and continue to provide backward power flow to the mode [as shown in Fig. 2(b)]. The SRR-TW structure can be therefore said to support a backward waveguide mode that is nearly isotropic in the xy plane.

The right-handed longitudinal harmonics $\mathbf{S}_{0,0,0}$ and $\mathbf{S}_{1,0,0}$ provide an uneven power distribution of forward waves propagating in opposite directions (resulting in a partial cancellation of right-handed power). These waves are distributed in k space at regular intervals with opposing power flow arising due to reflections off the lattice of inclusions. As the angle of propagation is changed from parallel to the x axis ($\phi = 0°$) to diagonally between the x and y axes ($\phi = 45°$), the lattice periodicity re-distributes the higher-order harmonic power from $\mathbf{S}_{1,0,0}$ to $\mathbf{S}_{1,0,0}$ and $\mathbf{S}_{0,-1,0}$ as shown in Fig. 2(a). For all angles of propagation, however, the net contribution of these components to the total power flow ranges is minor (less than 4% for $\phi = 0°$).

From this analysis, we can conclude that the negative refraction observed in SRR-TW metamaterial experiments is due to refraction of the right-handed free-space wave vector into the left-handed transverse harmonics. Furthermore, the presence of a strong fundamental harmonic ($\mathbf{S}_{0,0,0}$) yields a spatial spectral overlap with free space that enables mode matching to an incident or transmitted plane wave. This is consistent with the high transmittance observed in experiment with SRR-TW metamaterials.

IV. PHOTONIC CRYSTAL

Photonic crystal (PC) structures with strong periodic modulations in dielectric constant have also been shown to exhibit negative refraction of power at an interface [31,32]. In contrast to SRR-TW structures, PCs rely on band-folding to achieve negative refraction rather than double-negative effective parameters. It has been shown that a two-dimensional square lattice of silicon cylinders in air can support backward Bloch modes with noncircular EFCs (i.e., the fundamental wave vector $\mathbf{k}_{FB}$ and the averaged power flow $\mathbf{S}$ are not always collinear for all direction of propagation). Although this structure does indeed refract incident beams negatively, Lombardet *et al.* has shown through Fourier analysis that the refracted beam is a right-handed plane wave outside the first BZ, and that this behavior should be described through diffraction phenomenon rather than left-handedness [15].

Here, we apply the k-space analysis to a 2D photonic crystal composed of a dielectric containing a dense hexagonal (triangular) array of cylindrical holes. This crystal supports backward Bloch modes in all directions perpendicular to the holes and is an interesting case study for our analysis: unlike the structure in Ref. [15], it has circular EFCs that could be interpreted as corresponding to a two-dimensionally isotropic negative effective index [6,31,32]. In this photonic crystal, the holes have a diameter $2r = 0.8a$ and are arranged with a lattice constant a inside a dielectric medium of dielectric constant $\varepsilon = 12.96$. The two-dimensional rectangular unit cell of the structure [identified by the solid black lines in the inset of the Fig. 3(a)] has the width a and height $\sqrt{3}a$ along the x and y directions, respectively. By using this unit cell and applying periodic boundary conditions, the Bloch modes are solved for TE polarized waves (where the electric field lies perpendicular to the xy plane) at a normalized frequency $\Omega = a/\lambda_0 = 0.32$ and then expanded to its spatial-frequency harmonics. Figures 3(a) and 3(b) plot the power maps alongside the EFC contours of the structure for Bloch waves propagating along the symmetry axes ΓK and ΓM, respectively. Again, we can see that the $\mathbf{S}_{m,n}$ Poynting vectors are not necessarily normal to their corresponding EFCs. Although conventional EFC analysis would attribute backward power and observed negative refraction to an isotropic left-handed response, these power maps provide a completely different perspective. They reveal that backward modes are composed of right-handed TEM plane wave harmonics (where the Poynting vector and wave vector are parallel) in which the fundamental harmonic contributes negligibly to the total power. There are no left-handed components and backward power flow arises from right-handed higher-order harmonics, which propagate in the backward direction with respect to the fundamental Bloch wave vector. This insight reveals the right-handed origin of the observed negatively refracted beams
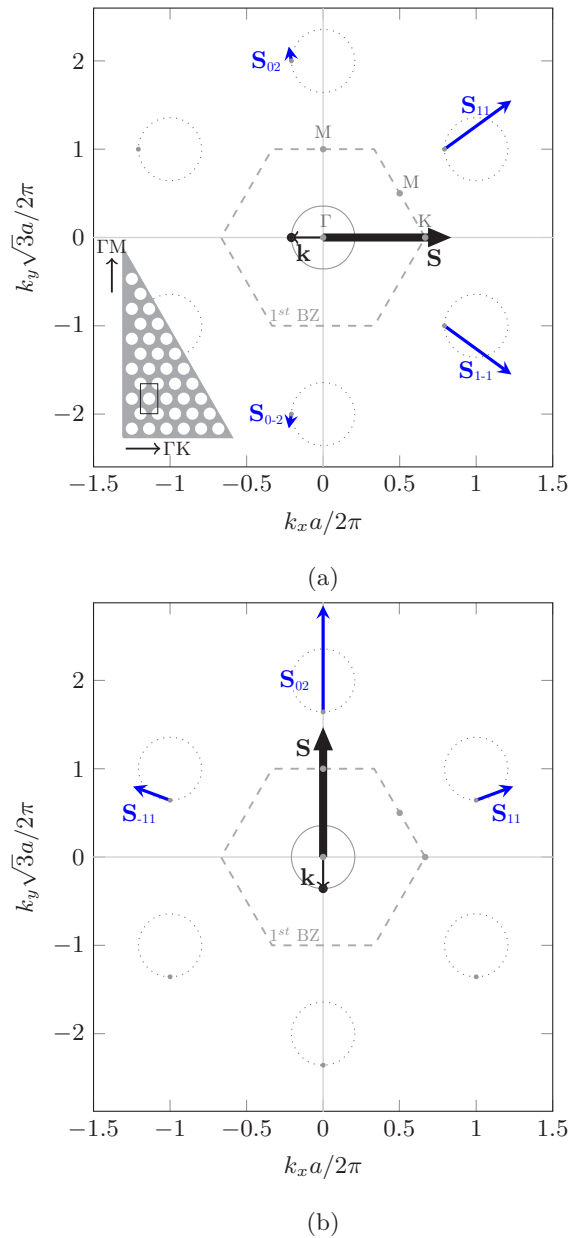
(a)

(b)

FIG. 3. The *k*-space diagrams for backward eigenmodes propagating along the (a) ΓK and (b) ΓM directions in the hexagonal photonic crystal. All Bloch harmonics for this structure are TEM right-handed plane waves plotted with blue arrows. The EFCs are given by the solid and dotted curves inside and outside the first BZ, respectively, where the first BZ is indicated by the light grey dashed hexagon. The photonic crystal geometry with its rectangular unit cell is illustrated in the inset. Again, as seen above, individual harmonic Poynting vectors are not restricted to being normal to the EFCs.

in photonic crystal prisms [24,32] and clearly demonstrates that an effective index should not be assigned to a periodic structure based solely on refraction observations. According to *k*-space power maps, Bloch modes in a periodic structure do not in general have a well-defined phase velocity, which therefore means that refraction beam angles cannot in general be related to a effective index of refraction in a consistent fashion.
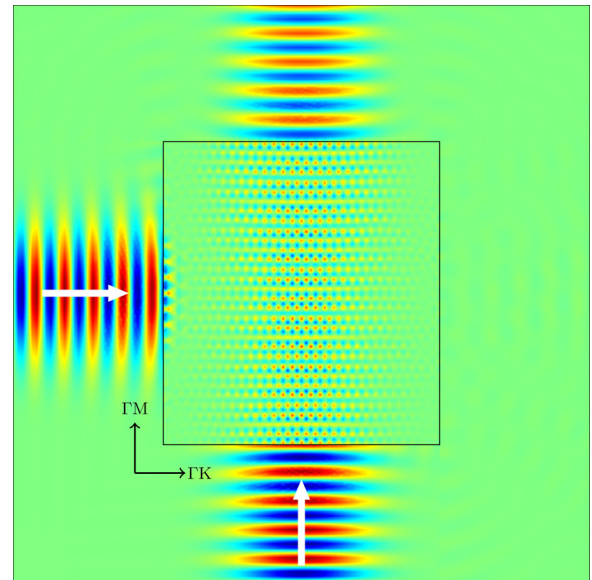
FIG. 4. The transverse electric field E_z is plotted for two Gaussian beams normally incident onto two different interfaces of a rectangular photonic crystal sample. The orthogonal incidence angles illustrate the different coupling efficiencies into the crystal. Note that both reflected beams have been omitted for clarity.

Figure 4 illustrates the transmission of Gaussian beams normally incident from free space onto two different interfaces of the photonic crystal [corresponding to the horizontal and vertical interfaces shown in the inset diagram of Fig. 3(a)]. Although the circular EFC of the photonic crystal would imply an isotropic response, the simulation results show a different transmission behavior at each interface. The beam propagating along the ΓK axis is almost completely reflected at the interface while the beam propagating along the ΓM axis shows high transmittance through the photonic crystal. This result is consistent with our *k*-space power maps once we recognize that the fundamental harmonic carries almost zero power (four orders of magnitude less than the total power). A plane wave incident along the ΓK axis has $k_y = 0$ and cannot phase match to a harmonic carrying any significant power, leading to poor coupling efficiency and high reflectivity. By contrast, a plane wave incident along the ΓM axis has $k_x = 0$ and can phase match to the dominant $S_{0,2}$ harmonic, thereby coupling strongly to a mode inside the photonic crystal.

These observations demonstrate that despite the presence of negative effective refractive index and circular EFC diagrams, an isotropic left-handed Veselago medium cannot truly describe the behavior of this photonic crystal. At this point, we must point out that the distribution of power across higher-order right-handed harmonics occurs for negatively refracting photonic crystals of all lattice spacings [18]. In other words, the *k*-space distribution does not change significantly when the unit cells are made extremely sub-wavelength and the medium enters what would typically be considered to be an effective medium regime. We will see in the following section that highly subwavelength crystals of magnetodielectric cylinders contain weak fundamental harmonics similar to those observed in photonic crystal structures.

V. SUB-WAVELENGTH MAGNETODIELECTRIC CRYSTAL

It has been shown that dense arrays of magnetodielectric subwavelength inclusions embedded in a host dielectric can support electric and magnetic resonances in the same frequency band and have been homogenized as double-negative media [7,12,33,34]. Here, we apply k-space analysis to a square two-dimensional crystal of nearly touching magnetodielectric cylinders in air which have been modeled by a two-dimensionally isotropic effective negative index $n = -1$. The cylinders are made of a magnetodielectric medium with $n = \varepsilon = \mu = 20$ and have a diameter $2r = 0.9a$, where a is the lattice constant of the crystal. This metamaterial supports backward Bloch modes under TM polarization (i.e. the magnetic field lies perpendicular to the xy plane) at the normalized frequency $\Omega = a/\lambda_0 = 0.0639$ for all angles of propagation in the xy plane. The corresponding power maps for propagation along the x axis ($\phi = 0°$) and along the diagonal ($\phi = 45°$) are illustrated in Figs. 5(a) and 5(b), respectively. Although backward power in this metamaterial structure has been attributed to an isotropic left-handed response, our power maps suggest that backward power actually arises from higher-order right-handed harmonics similar to the photonic crystal (as shown in Fig. 3).

A complete analysis of phase and power flow in this metamaterial therefore requires a harmonic expansion and cannot be modeled solely through an effective negative refractive index or EFC diagrams. A thorough k-space study of magnetodielectric crystals was presented in Ref. [18]. The details will not be repeated here, however, that study showed that power was carried in high-order right-handed harmonics (as in Fig. 5) regardless of how subwavelength the unit cell was made to be.

VI. SUBWAVELENGTH PLASMONIC CRYSTAL

A dense 2D array of metallic subwavelength cylinders has also been shown to support backward Bloch modes at optical frequencies in all directions of propagation perpendicular to the metallic cylinders [8,35]. This structure, known as a plasmonic crystal, operates below the plasma frequency of the metallic inclusions (with $\omega = 0.6\omega_p$) and has been shown to have a circular EFC with an inward pointing frequency gradient for TM polarized waves. Here we study a plasmonic crystal with a square lattice of metal cylinders embedded in air. The cylinders have a permittivity $\varepsilon_{metal} = -1.78\varepsilon_0$ and a diameter $2r = 0.9a$. At the normalized frequency $\Omega = a/\lambda_0 = 0.0954$, this metamaterial structure has been modeled as a two-dimensionally isotropic double-negative metamaterial.

The spatial frequency power maps of the structure are plotted in Figs. 6(a) and 6(b) for backward Bloch modes propagating parallel and diagonally to the lattice vectors, respectively. We can see from these diagrams that the concentrated fields surrounding the plasmonic cylinders resulted in power flow being distributed across many Bloch harmonics. Furthermore, we see that backward power arises from a combination of both right-handed and left-handed harmonics. The appearance of left-handed harmonic pairs (i.e., waveguide-mode pairs) with roughly isotropic behavior resembles the left-handed response
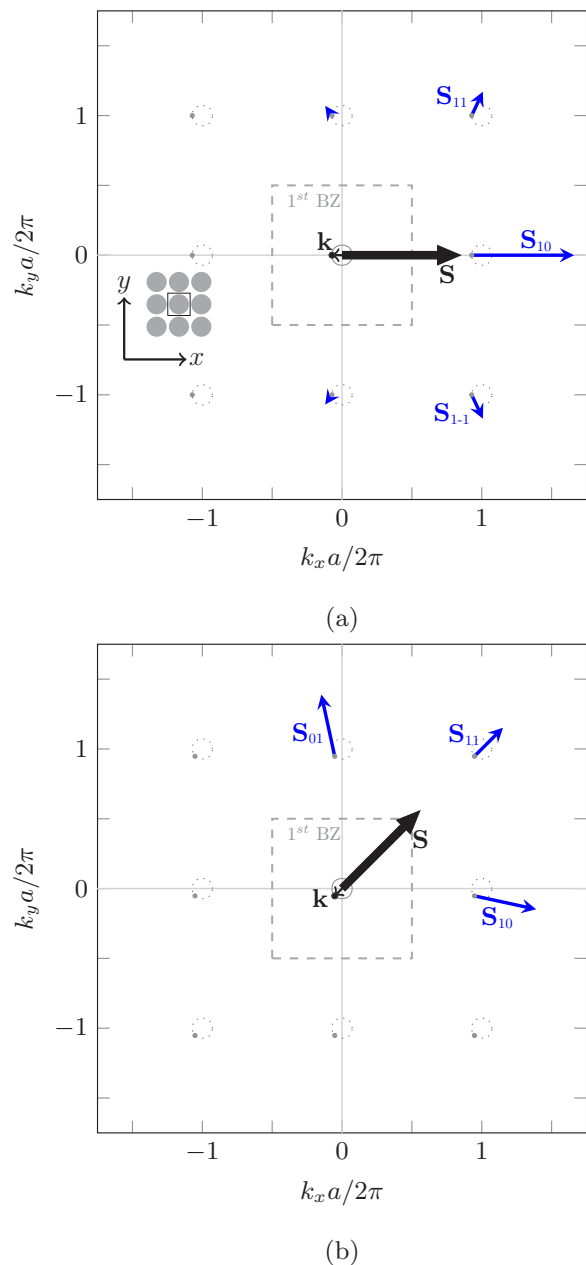

(a)

(b)

FIG. 5. The k-space illustration of Bloch harmonics for backward eigenmodes propagating in the magnetodielectric crystal (a) parallel to the x axis ($\phi = 0°$) and (b) diagonal to the x and y axes ($\phi = 45°$). The schematic geometry of the magnetodielectric crystal and the square unit cell are shown in the inset diagram.

of the SRR-TW metamaterial. Although the physical geometry of the plasmonic crystal strongly resembles that of a PC or an MD metamaterial, as do its EFCs and its homogenized effective refractive index, its electromagnetic behavior is very different. Instead of most of the power being contained in higher-order harmonics with large longitudinal wave vector components, the plasmonic crystals also have a strong fundamental and strong left-handed components adjacent to the first BZ. The presence of this strong fundamental implies that an external plane-wave can always phase-match to the plasmonic crystal modes, a conclusion consistent with the high transmittance through the plasmonic crystal lens observed in Ref. [35].
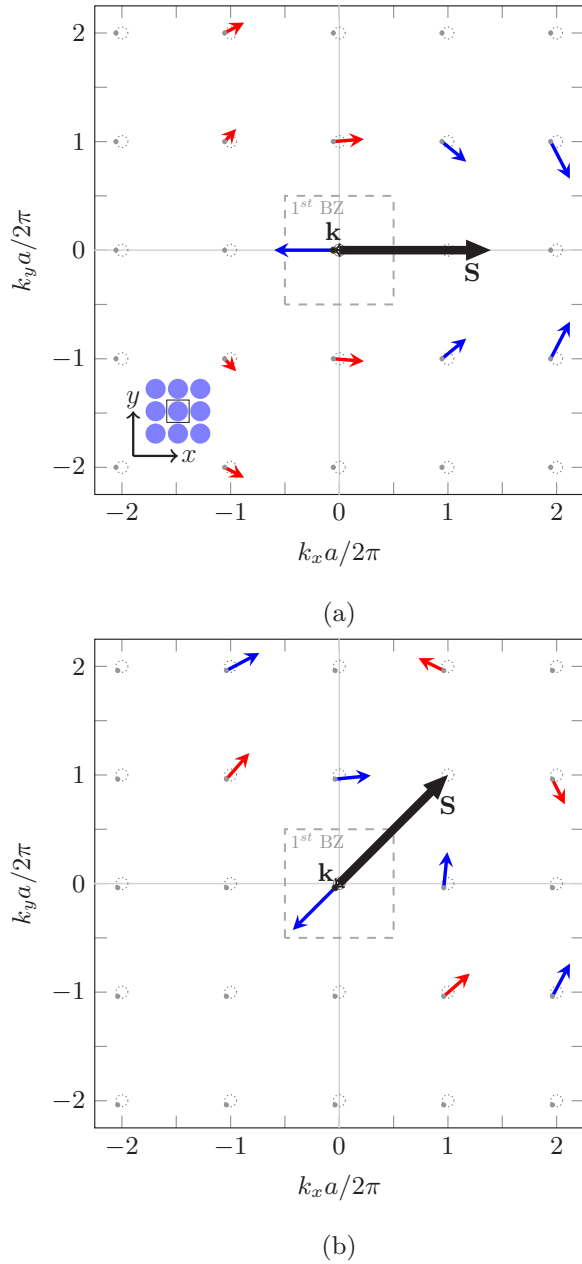
(a)

(b)

FIG. 6. The k-space illustration of Bloch harmonics for backward eigenmodes propagating in the plasmonic crystal (a) parallel to x axis ($\phi = 0°$) and (b) diagonally to x and y axes ($\phi = 45°$). Left-handed plane wave components are plotted with red arrows, while right-handed components are plotted with blue arrows. The schematic geometry of the plasmonic crystal and the square unit cell are shown in the inset.

VII. COUPLED-PLASMONIC-WAVEGUIDE METAMATERIAL

Metamaterials composed of stacked plasmonic waveguides can also support backward Bloch modes in all directions with roughly spherical backward-power EFCs at optical frequencies [9,36]. Here, we study one such metamaterial composed of a one-dimensional periodic repetition of five alternating thin layers of silver (Ag) and titanium dioxide (TiO$_2$), as illustrated in the inset of Fig. 7(b). The individual layers have thickness

(a)   (b)   (c)
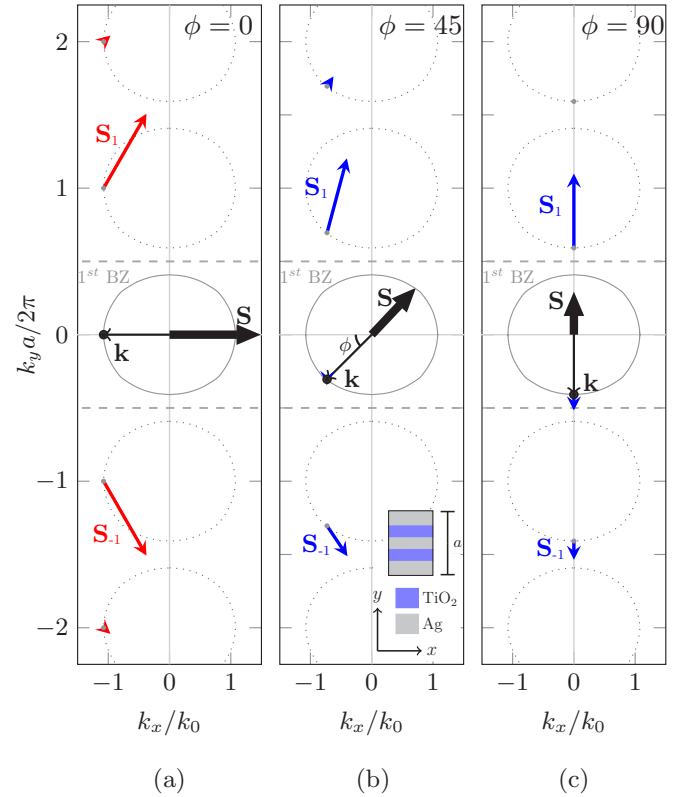
FIG. 7. The k-space illustration of Bloch harmonics for modes propagating in the coupled-plasmonic-waveguide metamaterial at an angle of (a) $\phi = 0°$, (b) $45°$, and (c) $90°$. As ϕ increases, dominant contributors to power flow shift from left-handed to right-handed plane-wave components. The schematic geometry of the unit cell is shown in the inset. Note that only the real parts of the complex eigenmodal wave vectors are drawn in the EFC diagrams. For a complete description of the complex wave vectors, the reader is referred to Ref. [17].

33, 28, 30, 28, and 33 nm, producing a total periodicity of $a = 152$ nm. This structure supports backwards Bloch waves in all directions under TM polarization at a wavelength of $\lambda_0 = 363.8$ nm (corresponding to a normalized frequency of $\Omega = a/\lambda_0 = 0.4178$) [9]. At this wavelength, the metamaterial layers were modeled using the complex permittivites $\epsilon_{Ag} = -2.522 + i0.251$ and $\epsilon_{TiO_2} = 7.835 + i0.392$ (nonmagnetic layers were considered).

Figure 7(a) shows the spatial-frequency power maps of the backward Bloch mode propagating along the layers ($\phi = 0°$). In this figure, the fundamental harmonic carries very little power and backward power arises primarily from the left-handed transverse harmonic pair. The presence of this left-handed waveguide mode in which power and phase propagate in opposite directions is consistent with the capability of planar plasmonic waveguides to support backward surface plasmon modes along their layers [37]. Since this medium is isotropic parallel to the layers (parallel to the xz plane), this left-handed response is sustained for all angles of in-plane propagation. Similarly to the SRR-TW metamaterial, the left-handed harmonic pairs rotate about the k_z axis to maintain isotropy.

However, as can be seen in Fig. 7, this left-handed response cannot be sustained for propagation across the layers (i.e. propagation anywhere in the xy plane). Figures 7(b) and 7(c) show

the k-space maps for propagation at an angle $\phi = 45°$ to the layers and normal to the layers ($\phi = 90°$). Unlike the case of in-plane propagation, the harmonics for these two propagation directions are all right-handed with a dominant high-order longitudinal harmonic $\mathbf{S}_1$ providing the greatest contribution to backward power. This response has strong similarities to those observed in photonic crystals and magnetodielectric media. Overall, the coupled-plasmonic-waveguide metamaterial demonstrates the usefulness of spatial frequency maps of power flow to differentiate between different types of backward modes and identify anisotropies that can be overlooked using traditional EFC analysis or effective medium theory.

A detailed study of coupling efficiency in Ref. [17] demonstrates the inherent deficiency of Bloch impedance in modeling the scattering behavior of the coupled-plasmonic-waveguide metamaterial. Although the Bloch impedance of the Bloch mode propagating along the layers in the metamaterial can be matched to a normally incident plane wave at an interface perpendicular to the layers, the lack of significant power in the fundamental harmonic results in a poor coupling efficiency. By contrast, tailoring the excitation to couple directly to the dominant harmonics can increase transmittance to 96%.

VIII. FISHNET METAMATERIAL

The final structure analyzed in this paper is the "fishnet" structure and is made of stacked metallic plates perforated by periodic hole arrays [38]. Here we study a simple structure in which perfectly conducting plates with zero thickness are stacked in air along the x axis with a periodicity $d = a/3$. The PEC screens are perforated with square holes of side length $b = a/3$ arranged in a square lattice of periodicity a. The unit cell is shown in the inset diagrams of Fig. 8(b). The Bloch modes were determined by applying PEC boundary conditions in the z direction (solid lines) and periodic boundary conditions along the x and y directions (dashed lines). Bloch modes propagating parallel to the xy plane were investigated at a normalized frequency of $\Omega = a/\lambda_0 = 0.95$ ($d/\lambda_0 = 0.317$).

In contrast to the periodic structures studied in previous sections, the EFC diagrams plotted in Fig. 8(a) are not circular and the fundamental wave vector $\mathbf{k}_{FB}$ and the time-and-space-averaged Poynting vector $\mathbf{S}$ (the frequency gradient) are only collinear (anti-parallel) for propagation normal to the plates (along the x axis). The spatial frequency power maps of the backward Bloch mode propagating along x axis are plotted in Fig. 8. In this figure, the fundamental harmonic is right handed and backward power arises primarily from the left-handed transverse harmonic pair (that once again form a backward waveguide mode). This resembles the k-space power maps of coupled-plasmonic-waveguide metamaterial for propagation along the layers and the left-handed response of SRR-TW and plasmonic crystal metamaterials.

IX. CONCLUSION

In this paper, we have shown how decomposing a backward Bloch mode into a complete set of spatial frequency harmonics can provide new insights into the behavior of metamaterials and other periodic structures that may otherwise be characterized by the same negative effective index of refraction.
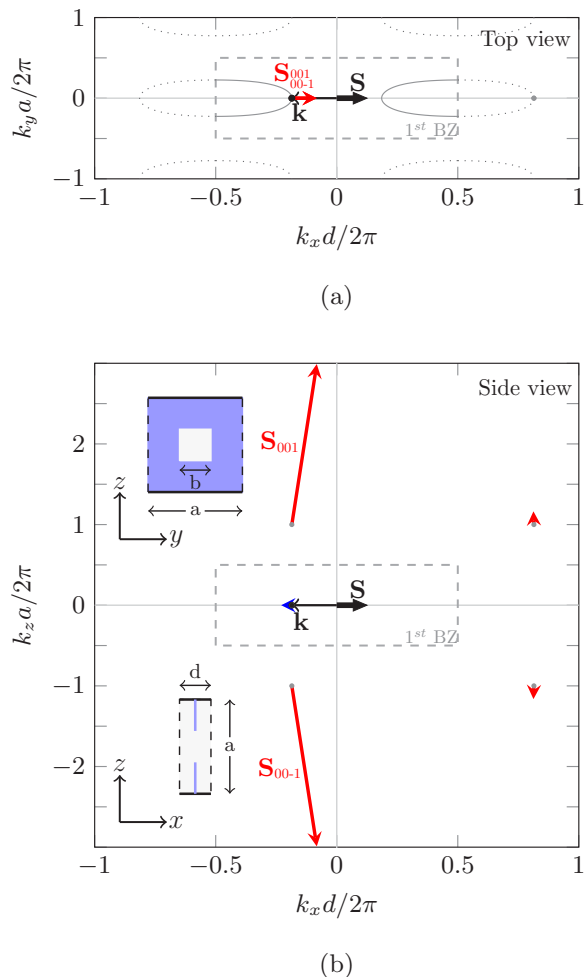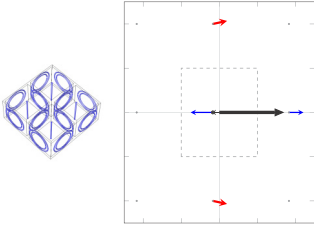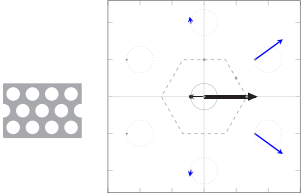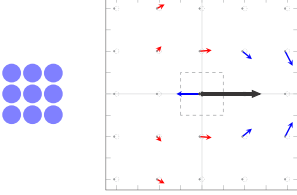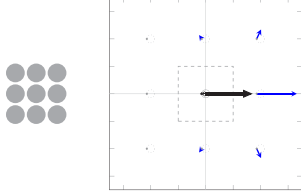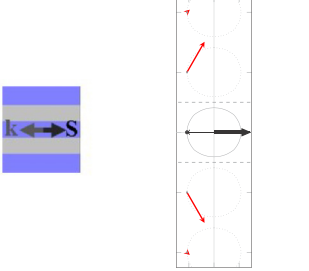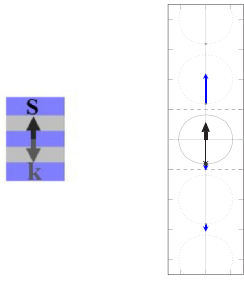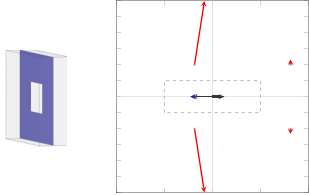

(a)

(b)

FIG. 8. The k-space illustration of Bloch harmonics (a) over the $k_x k_y$ plane (top view) and (b) over the $k_x k_z$ plane (side view) for a backward eigenmode propagating in the fishnet metamaterial along the k_x axis (normal to the perforated screens). The inset diagrams show the top view and side view of the unit cell in which the PEC screen and square hole are specified by the blue and white color, respectively. The PEC boundary conditions (solid lines) along the z axis and periodic boundary conditions (dashed lines) along the x and y axes have been applied in order to investigate propagation parallel to the xy plane.

Mapping power flow across the harmonics in k space reveals the phase and power relation (handedness) of each individual harmonic and provides a complete description of power and phase that is not available through effective medium theory or EFC analysis (repeated zone or otherwise). We have shown that although a medium may have (a) circular or spherical EFCs resembling that of an isotropic left-handed Veselago medium, (b) experimentally observed wide-angle negative refraction of electromagnetic beams, (c) negative effective parameters extracted through homogenization theory, and (d) subwavelength periodicity, these are not sufficient criteria for confirming an isotropic left-handed response and do not provide enough information to fully describe the electromagnetic behavior. We have shown that the spatial frequency origin of backward power flow can change with respect to the direction of propagation or from one periodic structure to another.

TABLE I. The categorization of periodic structures that support backward power across the electromagnetic spectrum based on their distinguishing feature in the spatial frequency domain.

The spatial frequency maps of power flow revealed that backward power arises through one of two basic mechanisms: either from pairs of left-handed transverse harmonics or from right-handed higher-order longitudinal harmonics. These spatial power maps provide an electromagnetic signature that can be used to identify and categorize periodic structures with similar dispersive behavior. In this work, we have shown that backward power arises from higher-order right-handed harmonics in structures such as photonic crystals, magnetodielectric crystals, and coupled-plasmonic-waveguide metamaterials (for propagation across their layers). Backward power is due to pairs of left-handed waveguide modes in SRR-TW composites, plasmonic crystals, fishnet structures (for on-axis propagation), and in coupled-plasmonic-waveguides metamaterials (for propagation along their layers). These results are summarized in Table I with all six structures classified into two groups. We also corroborated the hypothesis that k-space maps of power flow can provide information about the coupling efficiency into various metamaterials and be used to suggest incident wave excitation that provide enhanced transmission.

In summary, k-space analysis is shown to be a powerful tool to investigate metamaterials and photonic crystals (or any other periodic structures) and provide a simple visual representation of the complete relationship between phase and power flow. Using this tool, different structures across the electromagnetic spectrum can be easily compared and critical spatial spectral features identified. This method has been developed for bulk 3D periodic structures, however, it can be easily applied to planar metamaterials and metasurfaces to study the spatial spectral content of different surface modes and facilitate coupling to and from free space.

ACKNOWLEDGMENTS

[1] V. G. Veselago, Soviet Physics Uspekhi **10**, 509 (1968).

[2] J. B. Pendry, Phys. Rev. Lett. **85**, 3966 (2000).

[3] L. Brillouin, *Wave Propagation in Periodic Structures* (Dover, New York, 1953).

[4] P. J. B. Clarricoats and R. A. Waldron, J. Electron. Control **8**, 455 (1960).

[5] R. A. Shelby, D. R. Smith, S. C. Nemat-Nasser, and S. Schultz, Appl. Phys. Lett. **78**, 489 (2001).

[6] M. Notomi, Phys. Rev. B **62**, 10696 (2000).

[7] C. L. Holloway, E. F. Kuester, J. Baker-Jarvis, and P. Kabos, IEEE Trans. Antennas Propag. **51**, 2596 (2003).

[8] G. Shvets and Y. A. Urzhumov, J. Optics A **7**, S23 (2005).

[9] T. Xu, A. Agrawal, M. Abashin, K. J. Chau, and H. J. Lezec, Nature (London) **497**, 470 (2013).

[10] D. R. Smith, S. Schultz, P. Markoš, and C. M. Soukoulis, Phys. Rev. B **65**, 195104 (2002).

[11] M. G. Silveirinha, Phys. Rev. B **75**, 115104 (2007).

[12] A. Alù, Phys. Rev. B **84**, 075153 (2011).

[13] T. Paul, C. Menzel, W. Śmigaj, C. Rockstuhl, P. Lalanne, and F. Lederer, Phys. Rev. B **84**, 115142 (2011).

[14] A. Andryieuski, S. Ha, A. A. Sukhorukov, Y. S. Kivshar, and A. V. Lavrinenko, Phys. Rev. B **86**, 035127 (2012).

[15] B. Lombardet, L. A. Dunbar, R. Ferrini, and R. Houdré, J. Opt. Soc. Am. B **22**, 1179 (2005).

[16] I. Aghanejad, K. Chau, and L. Markley, in *2015 IEEE International Symposium on Antennas and Propagation USNC/URSI National Radio Science Meeting* (Vancouver, BC, Canada, 2015), pp. 657–658.

[17] I. Aghanejad, K. J. Chau, and L. Markley, Phys. Rev. B **94**, 165133 (2016).

[18] L. Markley, Phys. Rev. B **94**, 085108 (2016).

[19] K. Sakoda, *Optical Properties of Photonic Crystals*, 2nd ed. (Springer, New York, 2004).

[20] J. D. Joannopoulos, S. G. Johnson, J. N. Winn, and R. D. Meade, *Photonic Crystals: Molding the Flow of Light*, 2nd ed. (Princeton University Press, Princeton, 2008).

[21] C. Fietz, Y. Urzhumov, and G. Shvets, Opt. Express **19**, 19027 (2011).

[22] http://www.comsol.com

[23] J. T. Costa, M. G. Silveirinha, and A. Alù, Phys. Rev. B **83**, 165120 (2011).

[24] S. Foteinopoulou and C. M. Soukoulis, Phys. Rev. B **72**, 165112 (2005).

[25] R. Maas, E. Verhagen, J. Parsons, and A. Polman, ACS Photonics **1**, 670 (2014).

[26] D. R. Smith, W. J. Padilla, D. C. Vier, S. C. Nemat-Nasser, and S. Schultz, Phys. Rev. Lett. **84**, 4184 (2000).

[27] R. A. Shelby, D. R. Smith, and S. Schultz, Science **292**, 77 (2001).

[28] A. A. Houck, J. B. Brock, and I. L. Chuang, Phys. Rev. Lett. **90**, 137401 (2003).

[29] J. B. Pendry, A. J. Holden, D. J. Robbins, and W. J. Stewart, IEEE Trans. Microwave Theory Tech. **47**, 2075 (1999).

[30] J. B. Pendry, A. J. Holden, W. J. Stewart, and I. Youngs, Phys. Rev. Lett. **76**, 4773 (1996).

[31] S. Foteinopoulou and C. M. Soukoulis, Phys. Rev. B **67**, 235107 (2003).

[32] P. V. Parimi, W. T. Lu, P. Vodo, J. Sokoloff, J. S. Derov, and S. Sridhar, Phys. Rev. Lett. **92**, 127401 (2004).

[33] L. D. Landau, E. M. Lifshitz, and L. P. Pitaevski, *Electrodynamics of Continuous Media*, 2nd ed. (Pergamon Press, Oxford, 1984).

[34] X.-X. Liu and A. Al, Metamaterials **5**, 56 (2011).

[35] G. Shvets and Y. A. Urzhumov, Phys. Rev. Lett. **93**, 243902 (2004).

[36] E. Verhagen, R. de Waele, L. Kuipers, and A. Polman, Phys. Rev. Lett. **105**, 223901 (2010).

[37] J. A. Dionne, E. Verhagen, A. Polman, and H. A. Atwater, Opt. Express **16**, 19001 (2008).

[38] R. Marqués, L. Jelinek, F. Mesa, and F. Medina, Opt. Express **17**, 11582 (2009).